Journal of
Ship&Ocean
Technology
©DECEMBER 2003

SOTECH Vol. 7, No. 4, pp. 16~31, 2003

Calculation of Turbulent Flows around a Submarine for the Prediction of Hydrodynamic Performance

Jin Kim[1], Il-Ryong Park[1], Suak-Ho Van[1] and Wu-Joan Kim[2]

[1]Korea Research Institute of Ships & Ocean Engineering(KRISO), KORDI, Daejeon, Korea; E-mail: jkim@kriso.re.kr
[2]Dept. of Naval Architecture and Marine Eng., Mokpo National University, Mokpo, Korea;

Abstract

The finite volume based multi-block RANS code, WAVIS developed at KRISO, is used to simulate the turbulent flows around a submarine with the realizable k-ε turbulence model. RANS methods are verified and validated at the level of validation uncertainty 1.54% of the stagnation pressure coefficient for the solution of the turbulent flows around SUBOFF submarine model without appendages. Another SUBOFF configuration, axisymmetric body with four identical stern appendages, is also computed and validated with the experimental data of the nominal wake and hydrodynamic coefficients. The hydrodynamic forces and moments for SUBOFF model and a practical submarine are predicted at several drift and pitch angles. The computed results are in extremely good agreement with experimental data. Furthermore, it is noteworthy that all the computations at the present study were carried out in a PC and the CPU time required for 2.8 million grids was about 20 hours to get fully converged solution. The current study shows that CFD can be a very useful and cost effective tool for the prediction of the hydrodynamic performance of a submarine in the basic design stage.

Keywords: hydrodynamic force and moment, RANS, submarine

1 Introduction

The flow over a submarine is characterized by thick boundary layers, vortical flow structure generated by hull/appendage junctures and appendage turbulent wakes. In addition, highly three-dimensional turbulent shear flow including cross-flow separation is featured when the submarines are in maneuvering with non-zero drift angle or angle of attack.

It is a common practice to perform model tests to evaluate the hydrodynamic performance of a submarine in the basic design stage. However, the model test is usually expensive and time-consuming. Recently CFD (Computational Fluid Dynamics) techniques are utilized in many fluid engineering fields including ship design. Flow information around a hull and appendages, as well as integral quantities like force and moment, is very useful for the shape design of a submarine. If the CFD simulation is utilized for the evaluation of hydrodynamic performance prediction, it can help the submarine designer to produce the hull and appendage shape with the better performance. CFD can save a lot of efforts in measuring the global quantities and detailed flow information at

the towing tank or in the wind tunnel, although the computed results can't give the exactly same value as in the experiment. It is believed that CFD is the cost-effective tool for the performance prediction of a submarine.

The experimental measurements of the flow field from the DARPA SUBOFF submarine model were made in the Naval Surface Warfare Center Carderock Division (NSWCCD) (Groves et al 1989, Huang et al 1989, Ward and Growing 1990, Liu et al 1990, Blanton et al 1990, Growing 1990). A number of submarine configurations, ranging from axisymmetric body to a fully appended submarine, were constructed in order to provide CFD validation data. Several RANS simulations for these configurations were reported for the validation of their computation (Sheng et al 1995, Bull 1996). The present study covers the flow over the axisymmetric body at zero angle of attack and drift (designated as AFF-1-*) and axisymmetric body with four identical stern appendages (designated as AFF-3-*) at the level flight and several angle of attack for the validation of the RANS method.

More practical submarine geometry named Coelacanth II is considered. The hull form and appendages were designed by DAEWOO Shipbuilding & Marine Engineering Co., LTD. and the Vertical Planar Motion Mechanism (VPMM) test was performed at the Korea Research Institute of Ships & Ocean Engineering (KRISO) Towing Tank (Hwang et al 2002). Although this submarine is not actually built, the flow phenomena would be very similar to the real flow around the submarine of any navies. The calculations are carried out for zero, +/- 2^o, 4^o, 6^o, 8^o, 10^o, 12^o, 16^o of the angle of attack in vertical plane and drift angles in horizontal plane.

2 Computational method

The three-dimensional incompressible RANS code, WAVIS developed at KRISO/KORDI, is used for the present study. This code has been validated for an application to flow around the practical ship hull forms (Kim and Van 2000, Kim et al 2002).

2.1 Governing equations

The governing equations for turbulent flow in the present study are the Reynolds-Averaged Navier-Stokes equations for momentum transport and the continuity equation for mass conservation. The Cartesian coordinates are used, as shown in Figure 1, where (x, y, z) denotes downstream, starboard, and upward direction, respectively. The origin of the coordinates is located at the midship and the center of pressure hull. All the quantities are non-dimensionalized by the speed (U_∞) and the length (L) of a submarine, and fluid density (ρ). Continuity equation is

$$\frac{\partial u_k}{\partial x_k} = 0 \tag{1}$$

Momentum transport equations are

$$\frac{\partial u_i}{\partial t} + \frac{\partial (u_i u_j)}{\partial x_j} = -\frac{\partial p}{\partial x_i} + \frac{\partial \tau_{ij}}{\partial x_j} \tag{2}$$

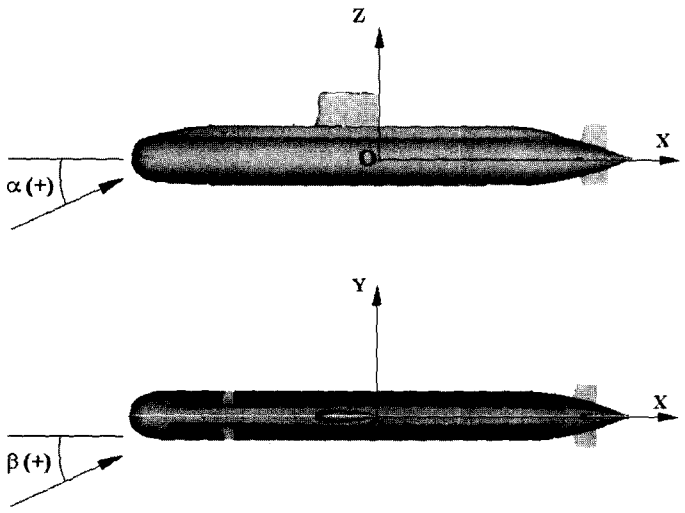

Figure 1: Coordinate systems

where u_i=(u, v, w) are velocity components in x_i=(x, y, z) directions, while p is static pressure. Stress tensor τ_{ij} can be written using Boussinesq's isotropic eddy viscosity hypothesis as follows.

$$\tau_{ij} = \nu_e(\frac{\partial u_i}{\partial u_j} + \frac{\partial u_j}{\partial u_i}) - \frac{2}{3}\delta_{ij}k \tag{3}$$

Here, k is turbulent kinetic energy and ν_e is effective viscosity, i.e., the sum of turbulent eddy viscosity(ν_t) and molecular kinematic viscosity(ν).

$$\nu_e = \nu_t + \frac{1}{Re} \tag{4}$$

and Re is Reynolds number ($U_\infty L/\nu$).

For turbulence closure, the realizable k-ε model (Shih et al 1995) is employed for the current study. This model showed better agreement for the application to the flow around practical ship hull forms (Kim and Van 2000, Kim et al 2002). With the k-ε turbulence model, the eddy viscosity ν_t can be usually written as

$$\nu_t = C_\mu \frac{k^2}{\varepsilon} \tag{5}$$

In the standard k-ε model C_μ=0.09. For the realizable model, C_μ has rather complicated form given in the followings.

$$C_\mu = \frac{1}{A_0 + A_S \frac{U^* k}{\varepsilon}} \tag{6}$$

where the terms are defined as

$$U^* = \sqrt{S_{ij}S_{ij} + \Omega_{ij}\Omega_{ij}} \tag{7}$$

$$S_{ij} = \frac{1}{2}\left(\frac{\partial u_i}{\partial x_j} + \frac{\partial u_j}{\partial x_i}\right) \tag{8}$$

$$\Omega_{ij} = \frac{1}{2}\left(\frac{\partial u_i}{\partial x_j} - \frac{\partial u_j}{\partial x_i}\right) \tag{9}$$

$$A_0 = 4.0, A_S = \sqrt{6}\cos\phi \tag{10}$$

$$\phi = \frac{1}{3}\arccos(\sqrt{6}W) \tag{11}$$

$$W = \frac{S_{ij}S_{jk}S_{ki}}{\tilde{S}^3}, \tilde{S} = \sqrt{S_{ij}S_{ij}} \tag{12}$$

The turbulent kinetic energy k can be obtained by the solution of the following transport equation.

$$\frac{\partial k}{\partial t} + \frac{\partial (u_j k)}{\partial x_j} = \frac{\partial}{\partial x_j}\left[\left(\nu + \frac{\nu_t}{\sigma_k}\right)\frac{\partial k}{\partial x_j}\right] + G - \varepsilon \tag{13}$$

where ε represents the dissipation rate of turbulent kinetic energy and G is production term as given below.

$$G = \nu_t\left(\frac{\partial u_i}{\partial x_j} + \frac{\partial u_j}{\partial x_i}\right)\frac{\partial u_i}{\partial x_j} \tag{14}$$

where the constant σ_k = 1.0 in (13).

The transport equation for dissipation rate ε is written by

$$\frac{\partial \varepsilon}{\partial t} + \frac{\partial (u_j \varepsilon)}{\partial x_j} = \frac{\partial}{\partial x_j}\left[\left(\nu + \frac{\nu_t}{\sigma_\varepsilon}\right)\frac{\partial \varepsilon}{\partial x_j}\right] + S_\varepsilon \tag{15}$$

For the realizable k-ε model,

$$S_\varepsilon = C_{\varepsilon 1} S\varepsilon - C_{\varepsilon 2}\frac{\varepsilon^2}{k + \sqrt{\nu\varepsilon}} \tag{16}$$

where σ_ε=1.2 , $C_{\varepsilon 2}$=1.9 , and

$$C_{\varepsilon 1} = \max\left(0.43, \frac{\eta}{\eta + 5}\right) \tag{17}$$

where $\eta = Sk/\varepsilon$.

It is advisory to use a near-wall turbulence model to resolve boundary layer up to the wall, however, the number of grid should be almost doubled. For the present study the so-called Launder and Spalding (1974)'s wall function is utilized to bridge the fully turbulent region and the wall. The first grid point in the wall function approach is approximately 100 times off the wall compared to that in the near wall turbulence model. It provides the economy and robustness to a viscous flow calculation method as a design tool. Since the flow around a ship is of the present interest, the so-called singular separation with flow reversal is not expected, although the formation of longitudinal vortex is often observed. The wall function is known to give good results for such a mild flow. The wall function adopted in the present calculation is given by

$$\frac{U_P C_\mu^{1/4} k_P^{1/2}}{\tau_w} = \frac{1}{\kappa}\ln(En_P^*) \tag{18}$$

$$\kappa = 0.41 \tag{19}$$

$$E = 8.342 \tag{20}$$

where τ_w is wall shear stress, U_P and k_P are the magnitude of velocity and turbulent kinetic energy at the center of the first cell off the wall. The non-dimensionalized normal distance from the wall n_P^* is given by

$$n_P^* = \frac{C_\mu^{1/4} k_P^{1/2} n_P}{\nu} \tag{21}$$

Generation of turbulent kinetic energy at the first cell off the wall is given as follows.

$$\bar{G}_P = \tau_w \left(\frac{\partial U}{\partial n} \right)_P = \frac{\tau_w^2}{\kappa C_\mu^{1/4} k_P^{1/2} n_P} \tag{22}$$

while dissipation at that cell is written by

$$\bar{\varepsilon}_P = \frac{C_\mu^{3/4} k_P^{3/2}}{\kappa n_P} \tag{23}$$

2.2 Numerical discretization

The cell-centered finite-volume method is utilized to discretize the governing equations, as discussed in Ferziger and Peric (1999). Governing equations are integrated over a grid cell Ω with boundary surface S, resulting in the following equations.

$$\int_S \vec{v} \cdot \vec{n} dS = 0 \tag{24}$$

$$\frac{\partial}{\partial t} \int_\Omega u_i d\Omega + \int_S u_i \vec{v} \cdot \vec{n} dS = \int_S \tau_{ij} \vec{i}_j \cdot \vec{n} dS - \int_S p \vec{i}_i \cdot \vec{n} dS \tag{25}$$

where $\vec{i}_j$ is unit vector in x_j-direction.

The first term of momentum transport equation, temporal derivative is ignored by putting very big time step, since only the steady solution is of the present interest. Convection terms are discretized using QUICK scheme of the third order. But the QUICK scheme requires 13 point stencil, resulting in complicated algebraic equations. Thus, the so-called deferred correction is adopted, which a simple upwind scheme is used with lagged higher-order terms. The deferred correction makes 7 point stencil with simple linear equations. Rewriting the third term of stress tensor,

$$\int_S \tau_{ij} \vec{i}_j \cdot \vec{n} dS = \int_S \nu_t \left(\frac{\partial u_i}{\partial x_j} + \frac{\partial u_j}{\partial x_i} \right) \vec{i}_j \cdot \vec{n} dS = \int_S \nu_t \left(grad(u_i) \cdot \vec{n} + \frac{\partial u_j}{\partial x_i} \vec{i}_j \cdot \vec{n} \right) ds \tag{26}$$

Central difference scheme is utilized for diffusion terms, while the terms coming from grid non-orthogonality are deferred. Linear equations obtained from 7 point stencil are solved using strongly implicit procedure (Stone 1968).

If the pressure field is known a prior, momentum equations will give correct velocity field. However, those velocity components will not satisfy the continuity equation. To ensure divergence-free velocity field, the SIMPLEC method (Van Doormal and Raithby 1984) is employed. Since the

collocated grid arrangement is chosen, the artificial dissipation term in pressure correction equation is added, as discussed in Rhie and Chow (1983). The resulting linear equations for pressure correction are solved using strongly implicit procedure until the equation residual drops by an order of magnitude each iteration.

With the generated grid system, flow calculation is initiated, starting from uniform stream. With the grids and initial guess for flow field ready, iteration begins for coupled partial differential equations. After three momentum-transport equations are solved sequentially to obtain preliminary velocity components, the pressure correction equations are solved to get pressure field. Then, velocity components are corrected using new pressure values. In the next turbulence equations are solved and eddy viscosity is updated. Iteration continues until total residuals of each momentum equation are less than 10^{-5}, which is about five orders less than the initial residuals.

3 RANS solutions for SUBOFF

3.1 SUBOFF experiments

The Submarine Technology Program (STP) Office of DARPA funded a concerted and coordinated CFD program to assist in the development of advanced submarines for the future. The SUBOFF project provides a forum for the CFD community to compare the numerical predictions of the flow field over an axisymmetric hull model with and without various typical appendage components with experimental data. The detail available data sets are well summarized by Liu and Huang (1998). Two SUBOFF models, DTRC model No. 5470 and 5471, were used. The two models differ only in the location of the surface pressure taps. Model 5470 was designed for the towing tank and Model 5471 for the wind tunnel. The details of the model configurations are described in Groves et al (1989).

Most measurements related to the level flights were performed at the wind tunnel with Model 5471. Figure 2 shows the dimensions of the wind tunnel and layout of the model. The flow was measured at the Reynolds number of 1.2×10^7. Eight basic model configurations (AFF-1 thorough 8) were tested at the wind tunnel. The measurement of the hydrodynamic forces and moments at various drift angles was conducted in the David Taylor Model Basin on a towing carriage utilizing a planar motion mechanism (PMM) with Model 5470 (Roddy 1990). All experiments in the towing tank were carried out at the Reynolds number of 1.4×10^7.

For the wind tunnel tests of each configuration, the pressure and wall shear stresses are measured on the hull surface. The measurement of the flow quantities are also performed along an axisymmetric body. They were the three components of mean velocities and their turbulence intensities, two Reynolds stresses, boundary layer surveys along the upper meridian at five locations, and wake survey. The uncertainty of the measurements was 2.5% of U_∞ for the mean velocity components and 0.2% for the Reynolds stresses, where U_∞ is the free stream inlet velocity. The uncertainty of the pressure and skin friction coefficients are ± 0.015 and ± 0.0002 for their values respectively.

For the towing tank test with PMM, the axial force coefficients are more difficult to measure accurately than the other coefficients and the experimental axial force coefficient data have 10% uncertainty. On the other experimental coefficients (vertical force and pitching moments) 5% of data uncertainty exist.

The present study covers the flow over the configuration AFF-1-*, the axisymmetric body

of revolution and the configuration AFF-3-*, axisymmetric body with four identical stern appendages.

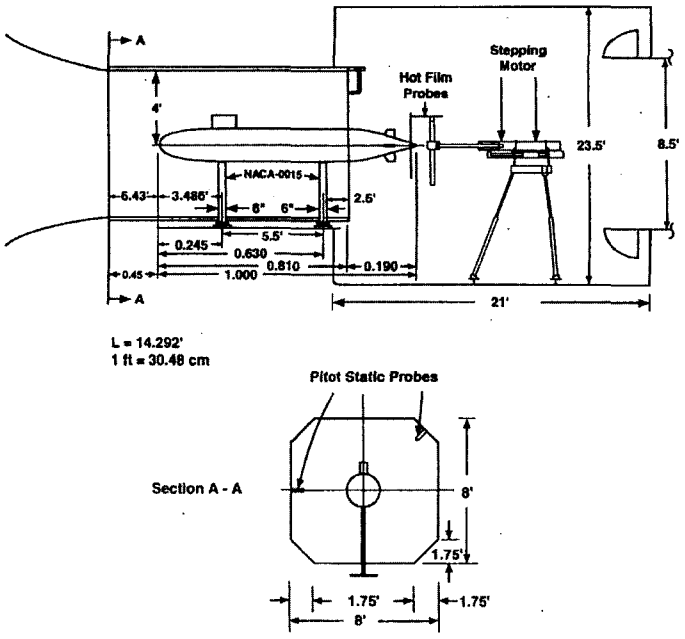

Figure 2: *Schematic view of experimental setup for SUBOFF model in the wind tunnel*

3.2 Verification & Validation (V&V) analysis and RANS solution for AFF-1 configuration

An assessment of the quality of the CFD result is imperative, which has accelerated progress on development of V&V methodology and procedure for estimating numerical and modeling errors and uncertainties in CFD simulations. However, in spite of progress, the various viewpoints have not yet fully converged and current methodology and procedure are not standardized. Here, however, the recommended V&V procedure are used, which is provided by Stern et al (2001).

In order to verify the RANS solution for the SUBOFF barehull (AFF-1-* configuration), three systematically refined grids are required. Non-integer grid refinement ratio $r_G = \sqrt{2}$ is selected in the present study. The fine grid is generated at first. Removing every second point in the fine grid can generate the coarse grid and the medium grid is generated by an interpolation method. The number of grids are 121 $\times$ 61 $\times$ 3 for the fine grid, 87 $\times$ 43 $\times$ 3 for the medium grid, and 61 $\times$ 31 $\times$ 3 for the coarse grid in the axial, radial and circumferential respectively. The number of grids in the circumferential direction is reduced to 3 by using symmetry condition. The realizable k-ε turbulence model is employed for the case of V&V analysis. Since the wall function is used, the distance of the first adjacent grid from the hull surface was adjusted to y^+=30-130 for the fine grid, 30-180 for the medium grid, and 30-250 for the coarse grid.

The pressure coefficient along the hull surface defined as $C_P = 2p/\rho U_\infty^2$ is selected as a point variable. The grid convergence for the pressure distribution along the hull surface is shown in Figure 3, including comparison with experimental data (Huang et al 1990). In their experiments,

the effect of tunnel blockage is notified. The square symbols imply their original measurements and the circle symbols are correction of the blockage effect.

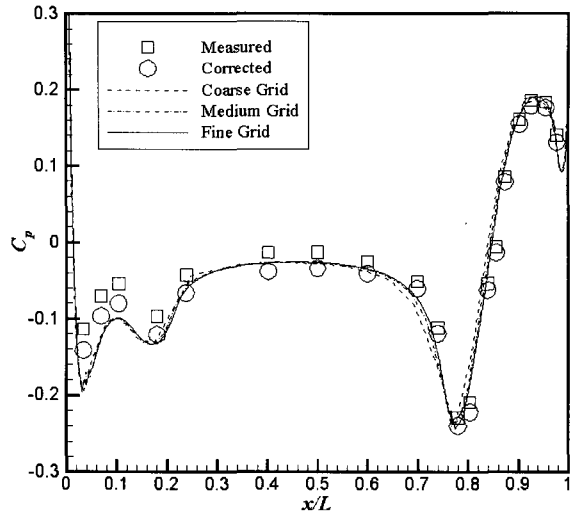

Figure 3: The grid convergence of the pressure coefficient profile along the full surface

To facilitate the V&V analysis, the solutions from all three grids are interpolated onto the same number of points with uniform spacing. The averaged L_2 norm value over interpolated values is used as a global metric. The definition of the averaged L_2 norm is as follows.

$$\|\mathbf{x}-\mathbf{y}\|_2 = \sqrt{\sum_{i=1}^{N}(x_i-y_i)^2}\Big/N \tag{27}$$

where **x**, **y** are the vector to compute the norm and x_i, y_i are their components. Thus, the separate L_2 norms of the solution change ε_{32} between the coarse and medium and ε_{21} between the medium and fine grids are used to define for the grid convergence ratioR_G, the estimated order of accuracy p_G, the correction factorC_G, and the grid uncertainty U_G in a profile-averaged sense. The detail derivations of these equations are given by Stern et al (2001).

$$\langle R_G\rangle = \|\varepsilon_{21}\|_2/\|\varepsilon_{32}\|_2 \tag{28}$$

$$\langle p_G\rangle = \frac{\ln\left(\|\varepsilon_{32}\|_2/\|\varepsilon_{21}\|_2\right)}{\ln(r_G)} \tag{29}$$

$$\langle C_G\rangle = \frac{r_G^{\langle P_G\rangle}-1}{r_G^{P_{G_{EST}}}-1} \tag{30}$$

$$\langle U_G\rangle = [2\,|1-\langle C_G\rangle|+1]\left|\frac{\|\varepsilon_{21}\|_2}{r_G^{\langle p_G\rangle}-1}\right| \tag{31}$$

where $\langle\rangle$ and $\|\,\|_2$ are used to denote a profile-averaged quantity (with ratio of solution changes based on L_2 norm) and L_2 norm, respectively. Based on the above equations, we get $\|\varepsilon_{32}\|_2$=

0.00164 and $\|\varepsilon_{21}\|_2$=0.00105. The number of interpolation points along the hull surface is varied, and so more than 20 points doesn't change much in L_2 norm value. 50 interpolation points are used in current analysis. Based on the above (28)-(30), the grid convergence ratio $\langle R_G \rangle$=0.64, order of accuracy $\langle p_G \rangle$=1.27, and correction factor $\langle C_G \rangle$=0.55 are calculated. Since $0 < \langle R_G \rangle < 1$, we can say the RANS solution is verified and has the monotonic convergence. The estimated grid uncertainty $\langle U_G \rangle$ from the (31) is 0.36% of the stagnation pressure coefficient ($C_P = 1.0$), which is less than the experimental data uncertainty $\langle U_D \rangle$, 1.5% of the stagnation pressure coefficient. The L_2 norm of the error $\|E\|_2$ of the fine grid solution compared to the experimental values is 0.51% of the stagnation pressure coefficient. The numerical simulation uncertainty U_{SN} can be defined as $\sqrt{U_G^2 + U_I^2}$, where U_I is the iterative uncertainty. When the solution is fully converged, the iterative uncertainty is usually negligible. Therefore, the numerical simulation uncertainty U_{SN} be equated to the grid uncertainty U_G. From the definition of the validation uncertainty $U_V = \sqrt{U_{SN}^2 + U_D^2}$, 1.54% of the stagnation pressure coefficient is obtained. Since $|E| < U_V$, the solution is globally validated at the level of $\langle U_V \rangle$=1.54% of the stagnation pressure coefficient.

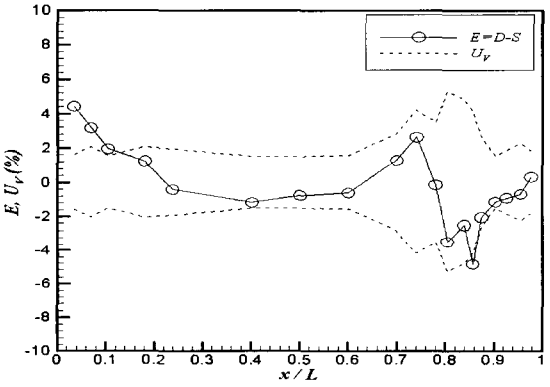

Figure 4: The distribution of error and validation uncertainty

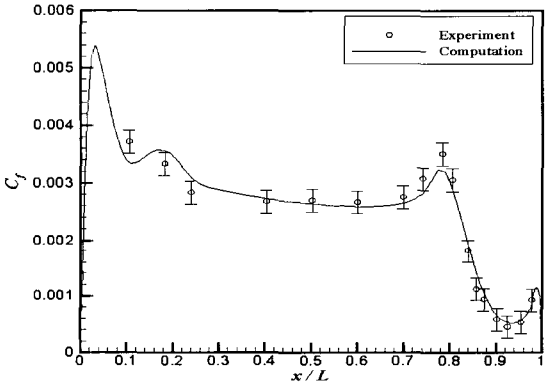

Figure 5: Comparisons of the computed and measured skin friction coefficients

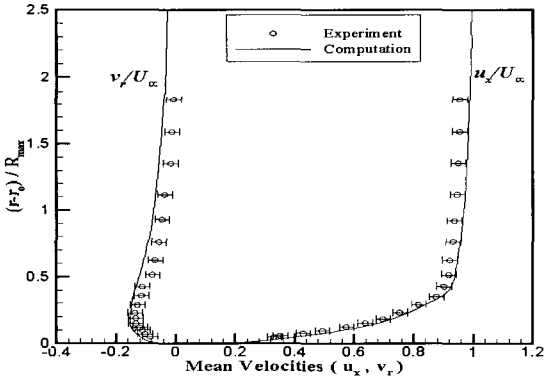

Figure 6: Comparisons of mean velocity profiles at x/L = 0.904

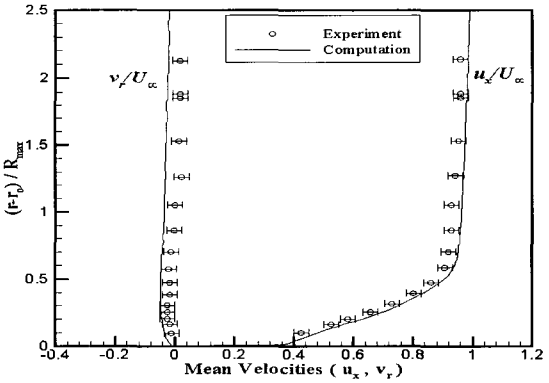

Figure 7: Comparisons of mean velocity profiles at x/L = 0.978

Distributions of the error and validation uncertainty, $(E, \pm U_V)$ are calculated similarly based

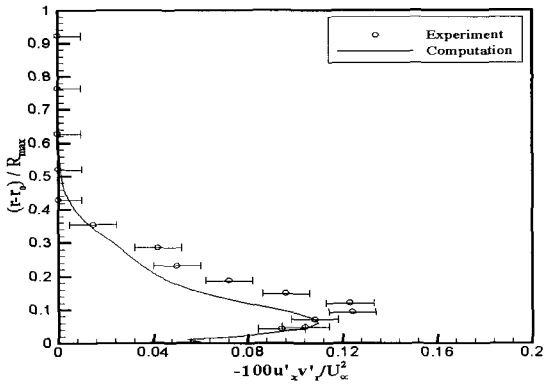

Figure 8: Comparisons of Reynolds stress profiles at x/L = 0.904

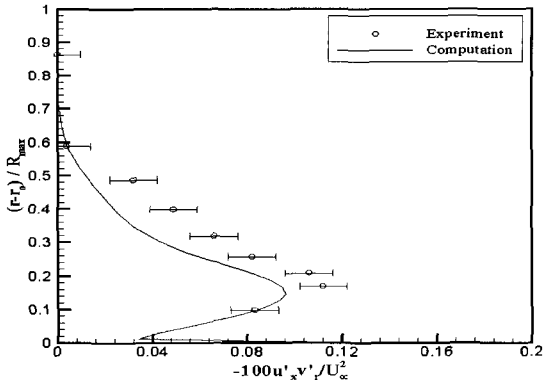

Figure 9: Comparisons of Reynolds stress profiles at x/L = 0.978

on the local solution changes ε_{32} and ε_{21} at the each axial point of the experimental data. Figure 4 shows the resulting distributions of $(E, \pm U_V)$. When E is within $\pm U_V$, the solutions are validated at the levels of U_V. The simulation errors for the fine grid solution are mostly located within the intervals of the validation uncertainty except for a couple of points in the region of forebody and the local maximum level of validation uncertainty is 5% of the stagnation pressure coefficient.

Therefore, the RANS solution for AFF-1 configuration of SUBOFF is verified and validated at the level of $\langle U_V \rangle$=1.54% of the stagnation pressure coefficient. The lack of validation comes from the underprediction of the local pressure coefficient near forebody compared to the experimental data.

Figure 5 shows the comparisons between the measured and computed skin friction coefficient, where computed results are performed with the fine grid. The measured data is given as symbols including the error bar representing the data uncertainty (±0.0002). The computed results are in good agreement with the experiment.

The computed mean velocity profiles at different axial locations, x/L = 0.904 and 0.978 are compared with the experiment data including the error bar representing the data uncertainty (±0.025) in Figure 6 and 7. The comparisons of the measured and computed Reynolds stresses $-\overline{u'_x v'_r}/U_\infty^2$ profiles are also shown in Figure 8 and 9 with the data uncertainty (±0.0001). Both computed mean velocity and Reynolds stress profiles show a fair agreement with the experimental data.

3.3 RANS solution for AFF-3 configuration

The turbulent flows around the axisymmetric body with four identical stern appendages (AFF-3-* configuration) at zero angle of attack are simulated with RANS method. The one side of y=0 plane is computed to reduce the number of grid using the symmetry condition. The number of grid in the axial direction is similarly kept with validated fine grid system for the previous barehull (AFF-1 configuration) solution.

Figure 10 displays the grid system used for this configuration, consisting of 24 blocks with about 1 million grid points. C-H type grid topology is used for the stern appendages. The distance of the first adjacent grid from the hull and appendage surface was adjusted to y^+=50-230.

Figure 11 displays the schematic view of the flow structures for this configuration. Each appendage generates two pairs of longitudinal vortices starting from the juncture of the hull and appendage (horseshe vortex) and tip trailing edge of the appendages. As a result, four distinct wake trails from four stern appendages are identified at the level flight with this configuration. Comparisons of measured and computed circumferential variation of axial velocities at x/L=0.978 and $r/R_{\max}$= 0.3 and 0.5 are shown in Figure 12. In the inner stern boundary layer ($r/R_{\max}$= 0.3), the axial velocities behind the appendages are clarified to be higher than those to each side of the appendage both in computation and measurement.

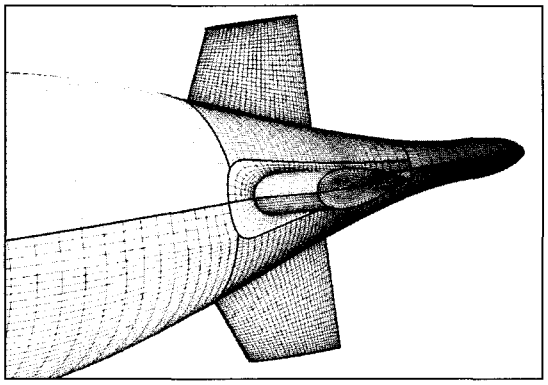

Figure 10: Surface mesh of the multi-block grid system for the AFF-3 configuration

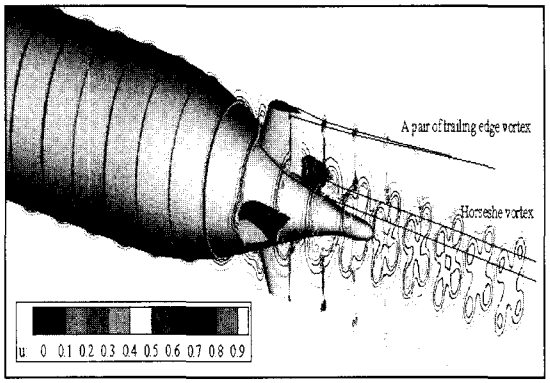

Figure 11: The schematic view of the flow structure with axial velocity contours

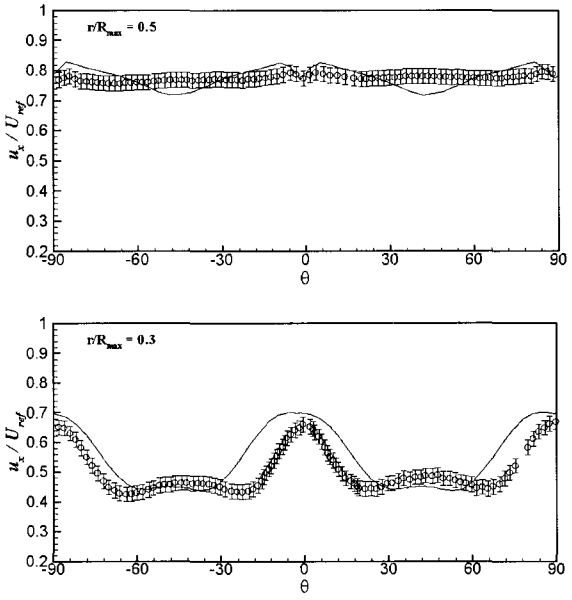

Figure 12: Wake survey comparisons at x/L=0.978

For the validation of the hydrodynamic coefficient predictions, the towing tank test (Model

5470) with PMM is simulated at the Reynolds number of 1.4×10^7 with zero, +/- 4°, 8°, 12°, 16° of the angle of attack (α) in vertical plane. Figure 13~15 show the comparisons of the axial, vertical forces and pitching moment coefficients with experimental data. Pitching moment is computed at LCB of the barehull (x/L = 0.4621) and the force and moments are non-dimensionalized by $0.5\rho L^2$ and $0.5\rho L^3$ respectively. The computed results are in extremely good agreement with experimental data.

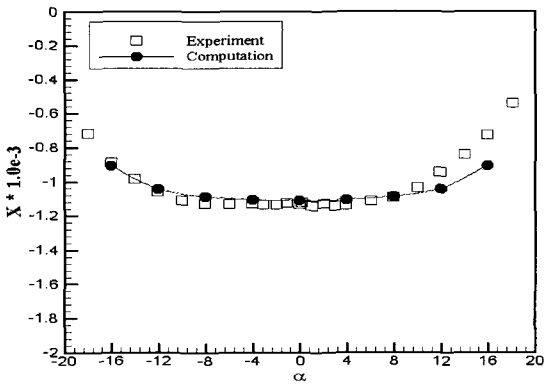

Figure 13: The axial force coefficients

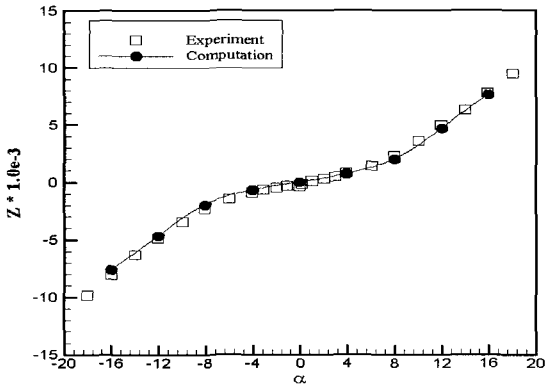

Figure 14: The vertical force coefficients

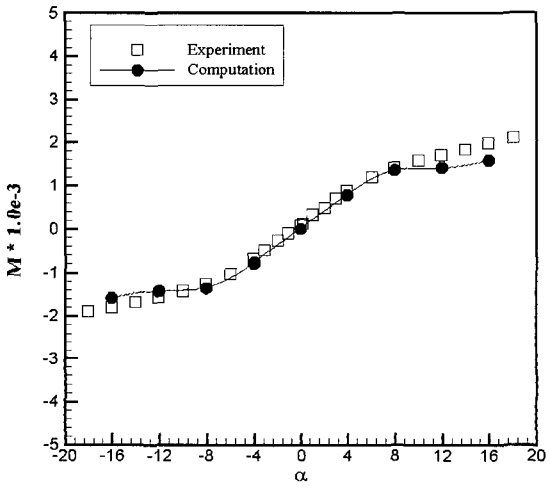

Figure 15: Pitching moment coefficients

4 Hydrodynamic performances for the practical submarine

DAEWOO Shipbuilding & Marine Engineering Co., LTD (DSME) designed 3000-ton class submarine hull forms named Coelacanth II including full appendages for the study of future development (Hwang et al 2002). Figure 16 shows the schematic view of the developed hull forms. The model test using the Vertical Planar Motion Mechanism (VPMM) was performed at the KRISO

Towing Tank in order to obtain the hydrodynamic coefficients for the simulation of 6-degree-of-freedom motion.

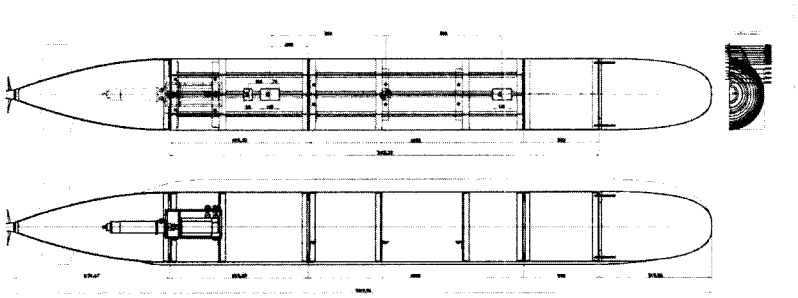

Figure 16: The schematic view of the hull forms of Coelacanth II

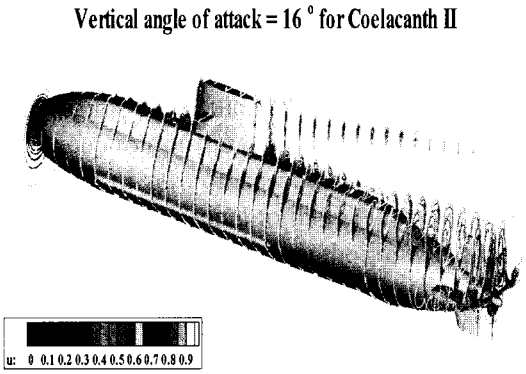

Figure 17: The schematic view of the flow structure with axial velocity contours

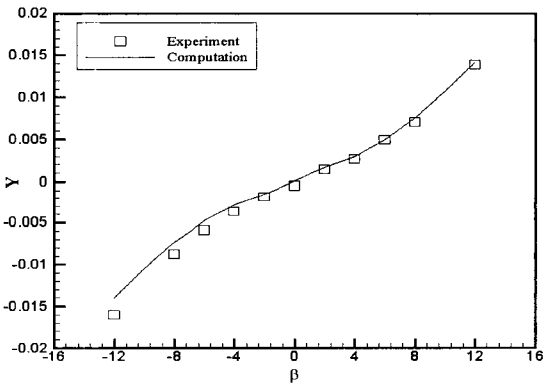

Figure 18: Lateral force coefficient

The hydrodynamic forces and moments for zero, +/- 2^o, 4^o, 6^o, 8^o, 10^o, 12^o, 16^o of the angle of attack in vertical plane and drift angles in horizontal plane are computed at the Reynolds number of 8.93×10^6, which corresponds to the model speed of 2.1252 m/s. For the vertical drift angle cases, the center plane of the submarine is considered as the plane of symmetry, thus, only the half in the starboard side is calculated and reflected. However, in the horizontal drift cases, both the port and the starboard side, i.e., the whole submarine is simulated. About 2.8 million grid points with 62 blocks are used for the whole domain simulation. Figure 17 displays complex flow structures at advance with 16^o vertical angle of attack. Boundary layer built along the hull surface is identified including strong flow separation on the hull surface.

The computed hydrodynamic force and moments are compared with experimental data carried out at KRISO towing tank. The lateral force (Y), yawing moment (N), and rolling moment (K) versus drift angles (β) are shown in Figure 18, 19, and 20 respectively. The vertical force (Z) and pitching moment (M) versus angle of attack (α) are shown in Figure 21 and 22. The present results shows a good agreement with the experimental measurements of the steady force and moments

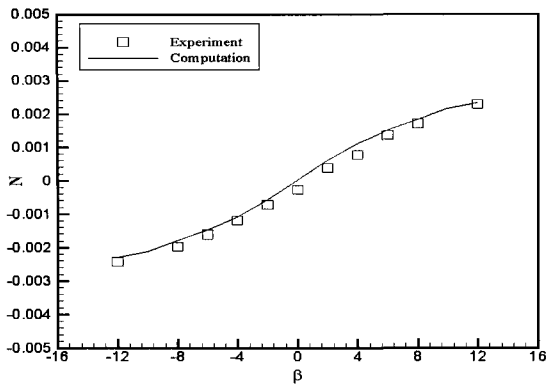

Figure 19: Yawing moment coefficient

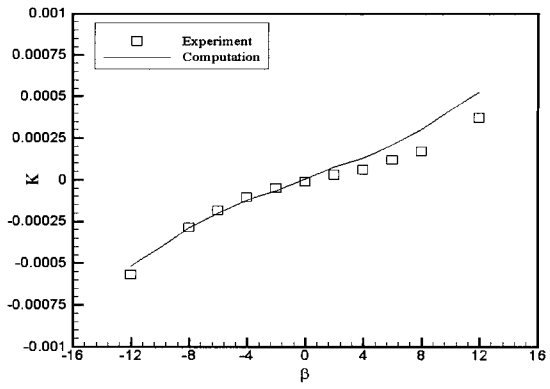

Figure 20: Rolling moment coefficient

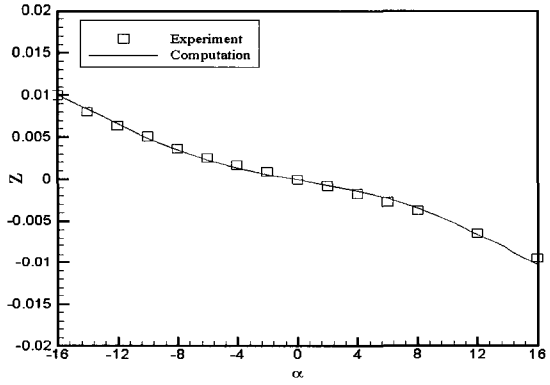

Figure 21: Vertical force coefficient

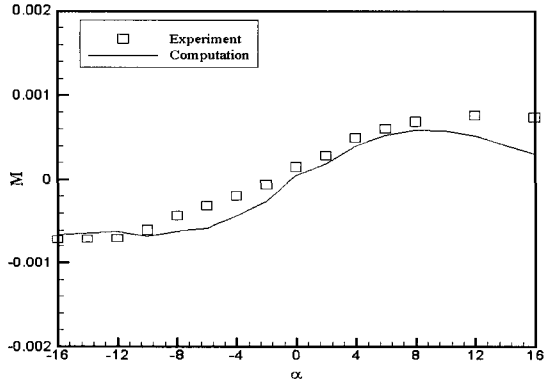

Figure 22: Pitching moment coefficient

acting on the practical submarine geometry, which are essential and foremost step in predicting the unsteady forces and moments acting on maneuvering submarines. The quality of agreement between the computation and experimental data is surprisingly good.

5 Summary and conclusions

The finite volume based multi-block RANS code, WAVIS developed at KRISO, is applied to the turbulent flows around a submarine configuration. RANS methods are verified and validated at the level of validation uncertainty 1.54% of the stagnation pressure coefficient for the solution of the turbulent flows around SUBOFF model without appendages. Another SUBOFF configuration, axisymmetric body with four identical stern appendages, is also computed and validated with the experimental data of the nominal wake and hydrodynamic coefficients. For the realistic application, the hydrodynamic forces and moments for a practical submarine (Coelacanth II) are predicted at several drift and pitch angles. The computed results are in extremely good agreement with experimental data.

It is noteworthy that all the computations in the present study were carried out in a PC and the CPU time required for 2.8 million grids was about 20 hours to get fully converged solution. The

cost and the level of flow details provided by CFD tools are drawing much attention for the shape design of hull forms and control plates. It is quite certain that CFD can be a very useful tool for the hydrodynamic performance prediction of submarine in the basic design stage.

Acknowledgement

This research was sponsored by the Ministry of Science and Technology (MOST), Korea under the dual use technology project and also supported by the basic research project at KRISO/KORDI.

References

BLANTON, J.N., FORLINI, T.J. AND PURTELL, L.P. 1990 Hot-film velocity measurement uncertainty for DARPA SUBOFF experiments. Report DTRC/SHD-1298-05

BULL, P. 1996 The validation of CFD predictions of nominal wake for the SUBOFF fully appended geometry. 21st Symposium on Naval Hydrodynamics, Trondheim, Norway, Aug.

FERZIGER, J.H. AND PERIC, M. 1999 Computational Methods for Fluid Dynamics, 2nd ed. Springer

GROVES, N.C., HUANG, T.T. AND CHANG, M.S. 1989 Geometric characteristics of DARPA SUBOFF models. Report DTRC/SHD-1298-01

GROWING, S. 1990 Pressure and shear stress measurement uncertainty for DARPA SUBOFF experiment. Report DTRC/SHD-1298-06

HUANG, T.T., LIU, H.L. AND GROVES, N.C. 1989 Experiments of DARPA SUBOFF program. Report DTRC/SHD-1298-02

HUANG, T.T., LIU, H.L., GROVES, N., FORLINI, T., BLANTON, J. AND GROWING, S. 1994 Measurements of flows over an axisymmetric body with various appendages in a wind tunnel: the DARPA Suboff experimental program. 19th Symposium on Naval Hydrodynamics, Washington, D. C., USA

HWANG, Y.S., LEE, S.W., YOON, J.D., RYU, M.C., KIM, I.H. AND SIN, M.S. 2002 On the development of hull forms and propeller for 3000-ton class submarine. Proc. of the Annual Autumn Meeting, SNAK, Busan, Korea, November, pp. 191-194

KIM, W.J., KIM, D.H. AND VAN, S.H. 2002 Computational study on turbulent flows around modern tanker hull forms. International Journal for Numerical Methods in Fluids, **38**, **4**, pp. 377-406.

KIM, W.J. AND VAN, S.H. 2000 Comparisons of turbulent flows around two modern VLCC hull forms. Proc. of a Workshop on Numerical Ship Hydrodynamics, Gothenburg, Sweden

LAUNDER, B.E. AND SPALDING, D.B. 1974 The numerical computation of turbulent flows. Comp. Meth. Appl. Mech. Eng., **3**, pp. 269-289

LIU, H.L., JIANG, C.W., FRY, D.J. AND CHANG, M.S. 1990 Installation and pretest analysis of DARPA SUBOFF model in the DTRC anechoic wind tunnel. Report DTRC/SHD-1298-04

LIU, H.L. AND HUANG, T.T. 1998 Summary of DARPA Suboff experimental program data. Report CRDKNSWC/HD-1298-11

RHIE, C.M. AND CHOW, W.L. 1983 A numerical study of the turbulent flow past an isolated airfoil with trailing edge separation. J. of AIAA, **21**, pp. 1525-1532

RODDY, R.F. 1990 Investigation of the stability and control characteristics of several configurations of the DARPA SUBOFF model (DTRC Model 5470) from captive model experiments. David Taylor Research Center Report DTRC/SHD-1298-08

SHENG, C., TAYLOR, L.K. AND WHITFIELD, D.L. 1995 Multiblock multigrid solution of three-dimensional incompressible turbulent flow about appended submarine configurations. AIAA Paper No. 95-0203, AIAA 33rd Aerospace Sciences Meeting and Exhibit, Reno, NV, January 9-12

SHIH, T.H., LIOU, W.W., SHABIR, A. AND ZHU, J. 1995 A new eddy viscosity model for high Reynolds number turbulent flows-model development and validation. Computers and Fluids, **24**, pp. 227-238

STERN, F., WILSON, R.V., COLEMAN, H. AND PATERSON, E.G. 2001 Comprehensive Approach to Verification and Validation of CFD Simulations - Part 1: Methodology and Procedure. J. of Fluids Engineering, **123**, **4**, pp. 793-802

STONE, H.L. 1968 Iterative solution of implicit approximations of multidimensional partial differential equations. J. of Numer. Anal., **5**, pp. 530-558

VAN DOORMAL, J.P. AND RAITHBY, G.D. 1984 Enhancements of the SIMPLE method for predicting incompressible fluid flows. Numerical Heat Transfer, **7**, pp. 147-163

WARD, K.C. AND GROWING, S. 1990 Hardware and instrumentation of the DARPA SUBOFF experiments. Report DTRC/SHD-1298-03